https://dx.doi.org/10.1016/j.tws.2017.10.009

Static strength of stainless steel K- and N-joints at elevated temperatures

Xiaoyi Lan [a, *], Yuner Huang [b], Tak-Ming Chan [a], Ben Young [c]

[a] Department of Civil and Environmental Engineering, The Hong Kong Polytechnic University, Hung Hom, Hong Kong, China

[b] School of Engineering, The University of Edinburgh, Edinburgh, Scotland, UK

[c] Department of Civil Engineering, The University of Hong Kong, Pokfulam Road, Hong Kong, China

*xiaoyi.lan@connect.polyu.hk

Abstract: This paper aims to investigate the static strength of stainless steel gap and overlapped K- and N-joints at elevated temperatures. A numerical parametric study was conducted on circular hollow section (CHS) K- and N-joints under axial loads in the braces at different temperatures ranging from 22 to 760°C. A wide range of geometric parameters and chord preload ratios of CHS K- and N-joints using duplex, high strength austenitic and normal strength (AISI 304) stainless steel was investigated. The joint strength reduction was compared with reduction factors of yield stress and elastic modulus of stainless steel materials at elevated temperatures. A unified strength equation for CHS K- and N-joints at elevated temperatures was proposed by adopting the reduction factor of yield stress. The statistical analysis shows that the proposed strength equation is accurate for stainless steel K- and N-joints at elevated temperatures.

Keywords: Circular hollow section; Elevated temperature; K-joint; N-joint; Stainless steel; Static strength

1. Introduction

Stainless steel tubular structures are increasingly popular due to their aesthetic appearance, improved resistance to fire and corrosion, and superior mechanical performance. Tubular joints are critical components in tubular structures because of their geometric discontinuity and high stress concentration at the connections. The structural behaviours and design of stainless steel tubular joints at ambient temperature have been investigated in recent years. Rasmussen and Young [1] and Rasmussen and Hasham [2] conducted tests on square hollow section (SHS) and circular hollow section (CHS) X- and K-joints using austenitic stainless steel 304L. Feng and Young [3-6] carried out experimental, numerical and theoretical investigations on rectangular hollow section (RHS) T- and X-joints using normal strength stainless steel (AISI 304) and high strength stainless steel (duplex and high strength austenitic). Huang and Young [7, 8] conducted experimental tests on ferritic stainless steel RHS T- and X-joints. However, mechanical properties of stainless steel materials in tubular structures experience significant deterioration in fire. The tubular joints are crucial for structural integrity. Therefore, it is important to investigate the structural performance of stainless steel tubular joints at elevated temperatures.

The joint strength at steady elevated temperatures is an important aspect of structural performance of tubular joints in fire. Tan et al. [9] and Shao et al. [10] conducted experimental tests and finite element analysis on carbon steel CHS T-joints under axial compression in the braces. It is found that design equations in EN 1993-1-8 [11], the CIDECT design guide [12] and API RP 2A WSD [13] replacing the steel yield stress at room temperature with that at elevated

temperatures may produce unconservative prediction of joint strength at elevated temperatures. However, the strength prediction of the design code and guide [11-13] may be conservative using the reduction factor of steel elastic modulus. Ozyurt et al. [14] carried out numerical study on carbon steel CHS and SHS tubular joints. It is found that the strength reduction of T-, Y- and X-joints under brace axial tension, and K- and N-joints under brace axial loads generally follows the reduction of steel yield stress at elevated temperatures. However, the strength reduction of T-, Y- and X-joints under brace axial compression follows more closely the reduction of steel elastic modulus. Xu [15] developed an artificial neural network model to predict the static strength of carbon steel CHS T-joints under brace axial compression in fire. Fung et al. [16] conducted test and numerical studies on the failure mechanism of CHS T-joints subjected to brace in-plane bending. It is observed that the failure mode of the joints is cracks forming along the weld toes at high temperatures and the effect of temperatures on joint strength reduction is significant. Shao et al. [17] presented a design method for the strength prediction of CHS K-joints at elevated temperatures based on a deforming rate criterion. Shao et al. [18] also numerically investigated the static strength of carbon steel CHS T-joints in fire obtained from steady and transient state analysis. Lan et al. [19] proposed an equation for predicting the joint strength reduction of internally ring-stiffened carbon steel CHS T-, Y- and DT-joints at elevated temperatures. Meanwhile, some studies on the fire resistance of carbon steel tubular joints under constant loading in fire have also been conducted. Yu et al. [20] conducted tests on carbon steel CHS T-joints after impact loading and found that the T-joints have minor change in fire resistance performance. Chen et al. [21] and Yang et al. [22] carried out experimental and numerical investigations on the failure mechanism of carbon steel CHS and SHS T-joints. It is shown that the T-joints failed by local yielding of chord wall around brace-chord intersection. He et al. [23-25] conducted experimental and numerical studies on carbon steel CHS gap K-joints and proposed a critical temperature method to assess the fire resistance performance of the K-joints. Gao et al. [26, 27] experimentally and numerically investigated the fire resistance of carbon steel CHS T-joints without and with reinforcement of collar plates and Y-joints. It is found that the fire resistance of the joints is improved by decreasing the load ratio. Chen et al. [28] conducted experimental and numerical studies on the fire resistance performance of internally ring-stiffened CHS T-joints and found that the internal rings could effectively enhance the fire resistance of the joints.

In contrast to the extensive studies on carbon steel tubular joints in fire, research on stainless steel tubular joints at elevated temperatures remains limited. Feng and Young [29] carried out numerical study on stainless steel RHS and SHS T- and X-joints, and proposed design equations for predicting the joint strength at elevated temperatures by modifying design equations in the CIDECT design guide [30]. Based on the comparison between the joint strength reduction and reduction factors of yield stress and elastic modulus of stainless steel materials, Lan and Huang [31] proposed a unified strength equation for stainless steel RHS, SHS and CHS T- and X-joints at elevated temperatures by introducing a temperature factor. However, there is a lack of research on stainless steel K- and N-joints at elevated temperatures.

This paper focuses on the static strength of stainless steel gap and overlapped CHS K- and N-joints under axial loads in the braces at elevated temperatures. A wide range of geometric parameters and different chord preload ratios of CHS K- and N-joints using duplex, high strength austenitic and normal strength (AISI 304) stainless steel were investigated. Based on the

comparison between the joint strength reduction and reduction factors of yield stress (0.2% proof stress) and elastic modulus of stainless steel materials, a unified strength equation for CHS K- and N-joints at elevated temperatures was proposed by adopting the reduction factor of yield stress of stainless steel materials.

2. Finite element model

2.1. General

The finite element (FE) software ABAQUS [32] was used to conduct the numerical analysis. It is noted that tests on steel tubular K- and N-joints at steady elevated temperatures are not available in existing literature. Tan et al. [9] conducted experimental tests on carbon steel CHS T-joints under brace axial compression at steady elevated temperatures. Lan et al. [19] successfully developed FE models which are capable of producing reasonably accurate predictions for the joint strengths in fire. In addition, Lan and Huang [31] also validated FE models of stainless steel X- and T-joints against the experimental and numerical joint strengths at room and elevated temperatures reported by Feng and Young [29]. It is also noted that tests on stainless steel tubular K- and N-joints at room temperature remain limited. Thus, the available test results of gap CHS K-joints using normal strength austenitic stainless steel (AISI 304) [2] and carbon steel [33], and completely overlapped N-joints using carbon steel [34, 35] at room temperature were used to validate the finite element models in this study. The joint parameters of the CHS K- and N-joints specimens are shown in Tables 1-2, including brace diameter (d_1 and d_2), brace wall thickness (t_1 and t_2) for gap K-joints, through brace diameter (d_1), through brace wall thickness (t_1), lap brace diameter (d_2), lap brace wall thickness (t_2) for overlapped N-joints, chord diameter (d), chord wall thickness (t), and angle between brace and chord members (θ_1 and θ_2). Other joint parameters not listed in Tables 1-2 are detailed in Rasmussen and Hasham [2], Kurobane et al. [33], Gho et al. [34] and Fung et al. [35]. The configuration and notations of the specimens are shown in Fig. 1.

2.2. Material properties

The adopted elastic modulus (E_0), yield stress (0.2% proof stress, f_y), ultimate stress (f_u) and ultimate strain at ultimate stress (ε_u) for the specimens [2, 33-35] are summarized in Table 3. The values of E_0, f_y and f_u reported by Rasmussen and Hasham [2] are adopted in developing the finite element models of stainless steel specimens KC48-30, KC48-45 and KC76-30. The values of ε_u and the corresponding stress-strain curves for specimens KC48-30, KC48-45 and KC76-30 are not reported in Rasmussen and Hasham [2], and thus they were obtained from the predictive equations for stainless steel materials proposed by Rasmussen [36]. The other three specimens (G2C [33], N-joint [34] and N-joint [35]) are in carbon steel materials. The values of f_y and f_u of specimen G2C are reported by Kurobane et al. [33], and thus adopted in developing the finite element model in this study. However, the values of E_0 and ε_u are not reported [33]. The adopted values of E_0 and ε_u in the FEM of specimen G2C were taken as 210 GPa and 10%, respectively, in accordance with those in Fleischer et al. [37] in which the adopted value of ε_u for S355, S460 and S690 steel is 10%. Only the values of E_0, f_y and f_u are reported in Gho et al. [34], and thus

the value of ε_u for N-joint [34] is also taken as 10% in this study. As the stress-strain curve was not reported in Kurobane et al. [33] and Gho et al. [34], a bi-linear stress-strain curve for carbon steel materials of specimens G2C [33] and N-joints [34] was adopted. Fung et al. [35] reported the values of E_0, f_y and f_u, and stress-strain curves, and therefore the reported material properties and stress-strain curves were adopted. It is noted that the measured value of ε_u for specimen N-joint [35] is also 10%. It is reasonable to assume that the value of ε_u for N-joint [34] is the same as those measured values of N-joint [35] as the steel materials used for N-joints in Gho et al. [34] and Fung et al. [35] are the same (API 5L Grade B steel). The Poisson's ratio of all steel materials equals to 0.3. The true stress (σ_T) and logarithmic plastic strain (ε_p) were converted from engineering stress (σ) and engineering strain (ε), and input in the FE models according to the recommendations of ABAQUS user's manual [32] as follows:

$$\sigma_T = \sigma(1+\varepsilon) \tag{1}$$

$$\varepsilon_p = \ln(1+\varepsilon) - \sigma_T / E_0 \tag{2}$$

where σ_T and σ are true and engineering stress, respectively, ε_p is logarithmic plastic strain, ε is engineering strain, and E_0 is elastic modulus.

2.3. Element type and mesh size

A four-node shell element S4R from ABAQUS library was adopted to model the brace and chord members. A five-point integration through the shell thickness was adopted. The mesh sizes of the brace and chord members were carefully determined by a mesh convergence study (sensitivity analysis). The adopted suitable mesh sizes for the gap K-joints [2, 33] and the intersection region between brace and chord members of the overlapped N-joints [34, 35] are shown in Table 4. A coarse mesh size of four times of the mesh size listed in Table 4 was used for regions near the end of brace and chord members of N-joints [34, 35].

Lee [38] points out that the gap size between brace members of CHS K-joints could have appreciable effect on the static strength of K-joints. EN 1993-1-8 [11], the CIDECT design guide [12] and API RP 2A WSD [13] adopt gap size functions, which are expressed as a function of ratio (g/t) of gap size (g) to chord wall thickness (t), to take such effect into account. It is noted that the static strength of CHS K-joints decreases with increasing gap size [11-13]. The effect of weld modelling on joint strengths largely depends on the discrepancy between the actual projected gap between the brace toes and the clear gap between the weld toes of CHS K-joints [38]. Thus, it is necessary to include weld modelling for CHS K-joints with a small gap size and a large weld size, as the large weld could significantly reduce the small gap size. It is noted that minimum ratios (g/t) for K-joints in Rasmussen and Hasham [2], and Kurobane et al. [33] is 8.6 and 3.8, respectively. Meanwhile the maximum ratio of weld size (t_w) to chord wall thickness (t) for K-joints in Rasmussen and Hasham [2] is 2.4. The weld size is not reported in Kurobane et al. [33]. The gap size is relatively large while the weld size is relatively small for the K-joints. Therefore, the weld modelling of the K-joints was not included in this study as discrepancy between the actual projected gap between the brace toes and the clear gap between the weld toes is not large. It is expected that the influence of excluding weld modelling on the joint strength will be minor according to the estimation from gap size functions [11-13]. The weld of CHS

N-joints was also excluded. The FE models without weld modelling adopted herein generally produce reasonably accurate and conservative predictions of joint strengths, as shown in Section 2.5.

2.4. Boundary condition and loading mode

For CHS K-joints, all degrees of freedom at the end of one brace of K-joints were restrained, except for the brace axial displacement and rotations in three directions, and the other brace end was fixed. One chord end was free to translate and rotate, and the other chord end was fixed. For CHS N-joints, all degrees of freedom at two brace ends were restricted, except for the brace axial displacement and three rotations at the end of the lap brace member. The two chord ends were fixed. The brace axial compression loading was applied by displacement at the brace end. The loads were applied in increments by using the "Static" method in ABAQUS library. Fig. 2 shows the adopted boundary condition and loading mode. The parameter of nonlinear geometry (*NLGEOM) was used to consider the effect of large displacement in the FE analysis.

2.5. Validation results

Fig. 3 shows the comparison of failure modes predicted by FE analysis with those observed in experimental tests [2, 34]. It is shown that the predicted failure modes of specimens KC48-30 [2] and N-joint [34] are chord face plastification and through brace face plastification, respectively, which are consistent with the test observations [2, 34, 39]. The comparison of load-displacement curves of specimens KC48-45 [2], G2C [14, 33] and N-joints [34, 35] obtained from experimental tests and FE analysis is shown in Fig. 4. The load and displacement denote the compression load applied at the brace end and corresponding brace axial displacement, respectively, except that the displacement for specimen KC48-45 refers to the relative displacement in the brace axial direction between positions near the brace end and in the middle line of chord side wall (see Fig. 6 in Rasmussen and Hasham [2] for details). It is shown that the adopted FE models could produce reasonably accurate prediction of load-displacement curves. The load-displacement curves of specimens KC48-30 and KC76-30 are not shown in Fig. 4, as the curves are not readily available (see Fig. 7(a) in Rasmussen and Hasham [2] for details). Table 4 shows the first peak loads obtained from FE analysis (N_{FE}) and experimental tests (N_{Test}). It is shown that the predicted loads agree with the test results well with maximum discrepancy of 10% of test loads [2, 33-35]. The mean value and coefficient of variation (COV) of the N_{FE}/N_{Test} ratio equal to 0.96 and 0.056, respectively. Thus, the FE models provide accurate and slightly conservative prediction for the peak loads of K- and N-joints in this study.

The validation study shows that the adopted FE models could produce reasonably accurate predictions of the failure mode, load-displacement curve and peak load of CHS K- and N-joints using stainless steel and carbon steel materials. Thus, the validated FE models will be used in the subsequent parametric investigation on CHS K- and N-joints at room and steady elevated temperatures by carefully incorporating the material properties of stainless steel materials at different temperatures.

3. Parametric study

3.1. General

An extensive numerical investigation on CHS K- and N-joints using duplex, high strength austenitic and normal strength (AISI 304) stainless steel at room and elevated temperatures was carried out. There are totally 400 specimens in parametric study, including 50 different joint configurations at 8 different temperatures ranging from 22 to 760°C. Static strengths of stainless steel K- and N-joints at eight different temperatures (i.e. 22, 80, 180, 320, 450, 550, 660 and 760°C) were obtained for each joint configuration. The joint parameters of gap K-joints (Fig. 5(a)), gap N-joints (Fig. 5(b)), and completely overlapped N-joints (Fig. 5(c)) are shown in Tables 5-6, including brace diameter (d_1 and d_2), brace wall thickness (t_1 and t_2), gap size between two brace members (g) for gap K- and N-joints, through brace diameter (d_1), through brace wall thickness (t_1), lap brace diameter (d_2), lap brace wall thickness (t_2), gap size between chord and lap brace (g) for completely overlapped N-joints, chord diameter (d), chord wall thickness (t), angle between brace and chord members (θ_1 and θ_2) and chord preload ratio (n). The notations for the joint parameters are shown in Fig 1. For gap K-joints, θ_1 is equal to θ_2, and θ_1 equals to 90° for gap and overlapped N-joints. The chord preload ratio (n) equals to the ratio of compressive chord preload (N_p) to chord yield load ($A_0 f_{y,T}$, where A_0 is chord cross-section area, and $f_{y,T}$ is steel yield stress at elevated temperatures).

The specimens were carefully designed to cover a wide range of joint parameters, including β ($=d_1/d$), β_b ($=d_2/d_1$), 2γ ($=d/t$), $2\gamma_b$ ($=d_1/t_1$), θ (θ_1 and θ_2) and n ($=N_p/A_0 f_{y,T}$). The ranges of joint parameter are $0.3\leq\beta\leq0.9$, $10\leq2\gamma\leq50$ and $0\leq n\leq0.6$ for gap K- and N-joints, $0.3\leq\beta_b\leq0.9$, $10\leq2\gamma_b\leq50$ and $0\leq n\leq0.6$ for completely overlapped N-joints, $30°\leq\theta_1\leq90°$ and $30°\leq\theta_2\leq60°$. It should be noted that the geometric parameters of the chord members of completely overlapped N-joints with sufficiently large gap sizes only have minor effect on the structural behaviour of the overlapped N-joints which fail by the most common failure mode i.e. through brace plastification [34, 35]. It is because the applied load in the lap brace is predominately transferred between the through brace and lap brace, and the failure occurs in the through brace members instead of the chord members. Thus, only chord preload ratio (n) of the chord members and geometric parameters (β_b, $2\gamma_b$ and θ_2) of the through brace members were investigated for the overlapped N-joints in this study. The chord length (l) is equal to 8 times of chord diameter ($l=8d$) to ensure that the stresses at the brace-chord intersection are not influenced by the chord ends [25]. The length of the through brace member is also equal to 8 times of through brace diameter ($l_1=8d_1$). The lengths of other brace members (l_1 and l_2) equal to 3 times of the brace diameter ($l_1=l_2=3d_1$) to avoid overall buckling of brace members, which could not reveal the true static strength of tubular joints. The specimen label of each tubular joint consists of three letters and one number. The first two letters (GK, GN or ON) indicate the joint type (gap K-joint, gap N-joint or overlapped N-joint). The third letter (D, H or N) refers to the stainless steel type, namely duplex, high strength austenitic and normal strength stainless steel, respectively. The number denotes the corresponding joint parameters, as shown in Tables 5-6. For example, OND1 represents completely overlapped N-joints using duplex stainless steel. The joint parameters of OND1 are listed in Table 6.

Material properties and stress-strain curves of stainless steel duplex, high strength austenitic (HSA), and normal strength (AISI 304) stainless steel at room and elevated temperatures [3, 4, 31, 40] were used in the finite element analysis. Table 7 shows the adopted material parameters

of stainless steel materials at room temperature, including elastic modulus (E_0), stress at plastic strain of 0.01% (f_p), yield stress (0.2% proof stress f_y), ultimate stress (f_u), and ultimate strain at ultimate stress (ε_u). The Poisson's ratio (v) equals to 0.3. It should be noted that the value of ultimate strain at ultimate stress at room temperature was obtained from the predictive equation proposed by Rasmussen [36]. The material parameters and stress-strain curves for duplex, high strength austenitic (HSA) and normal strength (AISI 304) stainless steel at different temperatures were obtained from the equations proposed by Chen and Young [40]. The true stress-strain curve converted from the engineering stress-strain curve was input in the FE models. A shell element S4R was used. A similar mesh sensitivity analysis as described in Section 2.3 for the K- and N-joints listed in Tables 5-6 was conducted. Suitable mesh sizes of 8 mm for the gap K- and N-joints, and 5 mm for the completely overlapped N-joints were adopted.

The boundary condition and loading mode of K- and N-joints for the parametric study are shown in Fig. 5. All degrees of freedom at the end of brace members were restrained, except for three rotations and brace axial displacement at the brace end under axial compression. The two ends of chord members were restrained from all degrees of freedom, except for axial displacement along chord member at one chord end. For K- and N-joints without chord preload, the axial compression in the brace was applied by displacement. For K- and N-joints with chord preload, the chord member was firstly preloaded, and then the brace end was loaded by displacement. It should be noted that the static strength of K- and N-joints is determined by the peak load or the load at a 3% indentation (i.e. indentation limit up to 3%d) in load-indentation curves. If the indentation at the peak load is smaller than the indentation limit, the peak load is considered to be the joint strength. If the indentation at the peak load is larger than the indentation limit, the load at the indentation limit is considered to be the joint strength. The indentation is defined as the difference of displacements at the crown position and point A on the chord side wall (Fig. 1), in order to exclude the global bending deformation of the chord member and to obtain localized deformation.

3.2. Results and analysis

The parametric study covered a wide range of geometric parameters ($0.3\leq\beta\leq0.9$, $10\leq2\gamma\leq50$, $0.3\leq\beta_b\leq0.9$, $10\leq2\gamma_b\leq50$, $30°\leq\theta_1\leq90°$ and $30°\leq\theta_2\leq60°$) and chord preload ratios ($0\leq n\leq0.6$). Different joint types (gap K-joint, gap N-joint and overlapped N-joint) and stainless steel types (duplex, high strength austenitic and normal strength stainless steel) were also studied. The ratio (R_T) of joint strength at elevated temperatures (N_T) to that at room temperature (N_0) was used to evaluate the effect of elevated temperatures on the static strength of K- and N-joints. The ratios (R_T) of specimens analysed in the parametric study are shown in Figs. 6-8. It should be noted that the investigated gap K- and N-joints failed by chord plastification and the failure mode of the overlapped N-joints was through brace plastification. Fig. 9 shows the failure modes (chord plastification and through brace plastification) of representative K- and N-joints at 760°C. The intersection regions in red became plastic. The comparison between ONN2 without chord preload (Fig. 9(c)) and ONN12 with chord preload ratio of 0.6 (Fig. 9(d)) indicates that the effect of chord preload on the structural behaviour of the overlapped N-joints is insignificant. It is because the chord remained intact under the axial loads in the chord and brace members, and the chord preload has minor effect on the failure occurring in the through brace members.

In general, the geometric parameters, chord preload ratios and stainless steel types have minor effect on the joint strength reduction (R_T) at elevated temperatures. However, the reduction of yield stress ($k_{y,T}$) and elastic modulus ($k_{E,T}$) of stainless steel at elevated temperatures has larger influence on the joint strength reduction. Similar findings that the effect of joint parameters on the joint strength reduction at elevated temperatures falls in a narrow range were reported by Ozyurt et al. [14] for carbon steel X-, T-, Y-, gap K- and N-joints, Lan et al. [19] for internally ring-stiffened carbon steel DT, T- and Y-joints, and Lan and Huang [31] for stainless steel X- and T-joints. Ozyurt et al. [14] also found that the joint strength reduction of carbon steel gap K- and N-joints generally follows the reduction of steel yield stress at elevated temperatures. Thus, the joint strength reduction (R_T) was compared with the reduction factors of yield stress ($k_{y,T}$) and elastic modulus ($k_{E,T}$) of duplex, high strength austenitic and normal strength stainless steel at elevated temperatures [40]. The equations proposed by Chen and Young [40] for $k_{y,T}$ and $k_{E,T}$ are as follows:

$$k_{y,T} = \frac{f_{y,T}}{f_{y0}} = a - \frac{(T-b)^n}{c} \tag{3}$$

$$k_{E,T} = \frac{E_T}{E_0} = a - \frac{(T-b)^n}{c} \tag{4}$$

where $f_{y,T}$ and f_{y0} are the yield stress at temperature T (°C) and room temperature, respectively, E_T and E_0 are the elastic modulus at temperature T and room temperature, respectively. The values of coefficients (a, b, c and n) in Eqs. (3-4) could be found in Chen and Young [40].

The comparison between the joint strength reduction and reduction factors of yield stress and elastic modulus of stainless steel at elevated temperatures for gap K-joints, gap N-joints and completely overlapped N-joints are shown in Figs. 6-8, respectively. The comparison shows that the reduction factors of yield stress ($k_{y,T}$) and elastic modulus ($k_{E,T}$) are generally the lower and upper bounds of the joint strength reduction (R_T), respectively, when the specimen temperature is lower than or equal to 350°C. The reduction factor of yield stress ($k_{y,T}$) is generally the lower bound of the joint strength reduction (R_T) of specimens at elevated temperatures ranging from 350 to 760°C. The joint strength reduction (R_T) generally follows the reduction of yield stress at elevated temperatures more closely.

4. Proposed design method

Based on the above observations, the reduction factor of stainless steel yield stress ($k_{y,T}$) is adopted to predict the joint strength reduction at different elevated temperatures. A unified strength equation for gap and overlapped CHS K- and N-joints using duplex, high strength austenitic and normal strength (AISI 304) stainless steel at elevated temperatures up to 760°C is proposed as follow:

$$N_T = k_{y,T} N_0 \tag{5}$$

where $k_{y,T}$ is the reduction factor of yield stress of stainless steel, N_T is the joint strength at elevated temperatures, N_0 is the joint strength at room temperature. The validity ranges of proposed strength equation are $0.3 \le \beta \le 0.9$, $10 \le 2\gamma \le 50$, $0.3 \le \beta_b \le 0.9$, $10 \le 2\gamma_b \le 50$, $30° \le \theta_1 \le 90°$,

341 $30° \le \theta_2 \le 60°$ and $0 \le n \le 0.6$. Figs. 6-8 show that the value of $k_{y,T}$ is generally the lower bound of the
342 joint strength reduction when the temperature is lower than or equal to 350°C and thus the
343 proposed strength equation (Eq. (5)) could produce lower and safe strength predictions for
344 specimens at temperatures lower than or equal to 350°C. The value of $k_{y,T}$ is reasonably accurate
345 for predicting the joint strength reduction (R_T) when the temperature ranges from 350 to 760°C
346 and thus Eq. (5) could produce reasonably accurate prediction of the joint strength at elevated
347 temperatures ranging from 350 to 760°C. The proposed unified strength equation is independent
348 of geometric parameters, chord preload ratios and stainless steel types of CHS K- and N-joints at
349 different elevated temperatures and only needs the calculation of the reduction factor of steel
350 yield stress. Thus, the proposed design method is simple and convenient to be used by engineers,
351 and it is also applicable for various types of steel tubular joints using different steel materials.
352 An error analysis was carried out to further assess the accuracy of the proposed strength
353 equation (Eq. (5)). The strength ratio (r_{si}) of the joint strength calculated from the proposed
354 strength equation (N_{ei}) to that obtained from finite element analysis (N_{fi}) was statistically
355 analysed for all specimens at elevated temperatures. The result of statistical analysis of r_{si} (=
356 N_{ei}/N_{fi}, i =1 to N, where N is the number of specimens at elevated temperatures analysed in each
357 case) is summarised in Table 8. The relative error (e_i), the average relative error (e) and relative
358 standard deviation (s) are as follows:

$$e_i = \frac{N_{fi} - N_{ei}}{N_{fi}} (i = 1, 2, 3, ..., N) \tag{6}$$

$$e = \frac{\sum_{i=1}^{N} | e_i |}{N} \tag{7}$$

$$s = \sqrt{\frac{\sum_{i=1}^{N} | e_i |^2}{N-1}} \tag{8}$$

359 Table 8 shows that the mean value of the strength ratio (r_{si}) is close to unity (i.e. 0.98 for gap
360 K- and N-joints, and 0.96 for overlapped N-joints), and the values of e and s are lower than
361 4.58% and 5.39%, respectively, for K- and N-joints. Such values therefore indicate that the
362 proposed strength equation could produce reasonably accurate and conservative prediction of the
363 joint strength at elevated temperatures.
364 A unified equation for predicting the static strength of gap and overlapped stainless steel CHS
365 K- and N-joints (N_T) at elevated temperatures was proposed by introducing the reduction factor
366 of steel yield stress ($k_{y,T}$) to the joint strength at room temperature (N_0). The joint strength at
367 room temperature was obtained from numerical simulations in this study, as there are no accurate
368 strength equations for stainless steel K- and N-joints at room temperature in the literature.
369 Therefore, further research is needed to propose design rules for the determination of static
370 strength of stainless steel K- and N-joints at room temperature (N_0). Furthermore, the failure
371 modes investigated in this study were chord plastification for the gap K- and N-joints and
372 through brace plastification for the overlapped N-joints. The failure mode of local buckling of
373 brace members under axial compression was not investigated as such failure could be prevented
374 by adopting Class 1 or 2 cross-sections [11-13]. Chord punching shear failure was also not
375 included in this study as such failure mode could not be well simulated by the adopted finite

element models. Further investigation is needed to examine whether the proposed design method is also applicable for the failure mode of punching shear.

5. Conclusions

This paper presents a numerical parametric study on the static strength of gap and overlapped CHS K- and N-joints using duplex, high strength austenitic and normal strength stainless steel under axial loads in the braces at elevated temperatures. The parametric study covered a wide range of parameters including the geometric parameter, chord preload ratio, and stainless steel type. The joint strength reduction was compared with the reduction factors of yield stress and elastic modulus of stainless steel at elevated temperatures. The major findings are as follows:

(1) The joint geometric parameter, chord preload ratio and stainless steel type have minor effect on the *joint strength reduction* of stainless steel CHS K- and N-joints at elevated temperatures. The joint strength reduction generally follows closely the reduction of yield stress of stainless steel at elevated temperatures.
(2) A unified strength equation for stainless steel CHS K- and N-joints at elevated temperatures was proposed by adopting the reduction factor of yield stress of stainless steel materials. The statistical analysis shows that the proposed strength equation (Eq. (5)) is reasonably accurate.

6. Acknowledgements

The authors appreciate the support from the Chinese National Engineering Research Centre for Steel Construction (Hong Kong Branch) at the Hong Kong Polytechnic University. The first author is also grateful for the support given by the Research Grants Council of Hong Kong for the Hong Kong PhD Fellowship Scheme.

References

[1] Rasmussen KJR, Young B. Tests of X- and K-joints in SHS stainless steel tubes. J Struct Eng 2001; 127(10):1173-1182.
[2] Rasmussen KJR, Hasham AS. Tests of X- and K-joints in CHS stainless steel tubes. J Struct Eng 2001; 127(10):1183-1189.
[3] Feng R, Young B. Experimental investigation of cold-formed stainless steel tubular T-joints. Thin-Walled Struct 2008; 46(10):1129-1142.
[4] Feng R, Young B. Tests and behaviour of cold-formed stainless steel tubular X-joints. Thin-Walled Struct 2010; 48(12):921-934.
[5] Feng R, Young B. Design of cold-formed stainless steel tubular T- and X-joints. J Constr Steel Res 2011; 67:421-436.
[6] Feng R, Young B. Theoretical analysis of cold-formed stainless steel tubular joints. Eng Sruct 2015; 83:99-115.
[7] Huang Y, Young B. Experimental investigation of cold-formed ferritic stainless steel tubular T-joints, in: Proceedings of the Eighth International Conference on Advances in Steel Structures, Lisbon, 2015.

[8] Huang Y, Young B. Experimental investigation of cold-formed ferritic stainless steel tubular X-joints, in Proceedings of the International Colloquium on Stability and Ductility of Steel Structures, Timisoara, 2016.
[9] Tan KH, Fung TC, Nguyen MP. Structural behaviors of CHS T-joints subjected to brace axial compression in fire conditions. J Struct Eng 2013; 139: 73-84.
[10] Shao YB, Zheng YJ, Zhao HC, Yang DP. Performance of tubular T-joints at elevated temperatures by considering effect of chord compressive stress. Thin-Walled Struct 2016; 98: 533-546.
[11] Eurocode 3 (EC3), Design of steel structures-Part 1-8: Design of joints. European Committee for Standardization, EN 1993-1-8, CEN. Brussels, 2005.
[12] Wardenier J, Kurobane Y, Packer JA, van der Vegte A, Zhao XL. Design guide for circular hollow section (CHS) joints under predominantly static loading. CIDECT, Verlag TUV Rheinland. Cologne, Germany, 2008.
[13] American Petroleum Institute (API), Recommended Practice for Planning, Designing and Constructing Fixed Offshore Platforms-Working Stress Design. API Recommended Practice 2A WSD (RP 2A WSD). Washington DC, 2000.
[14] Ozyurt E, Wang YC, Tan KH. Elevated temperature resistance of welded tubular joints under axial load in the brace member. Eng Struct 2014; 59: 574-586.
[15] Xu JX, Zhao JC, Song ZS, Liu ML. Prediction of ultimate bearing capacity of Tubular T-joint under fire using artificial neural networks. Safety Sci, 2012; 50(7): 1495-1501.
[16] Fung TC, Tan KH, Nguyen MP. Structural behavior of CHS T-joints subjected to static in-plane bending in fire conditions. J Struct Eng, 2015; 142(3): 04015155.
[17] Shao YB, He SB, Yang DP. Prediction on static strength for CHS tubular K-joints at elevated temperature. KSCE J Civ Eng, 2017, 21(3): 900-911.
[18] Shao YB, Zhao HC, Yang DP. Discussion on two methods for determining static strength of tubular T-joints at elevated temperature. Adv Struct Eng 2016: 1369433216662287.
[19] Lan XY, Wang F, Luo ZF, Liu DD, Ning C, Xu XF. Joint strength reduction factor of internally ring-stiffened tubular joints at elevated temperatures. Adv Struct Eng 2016; 19(10): 1650-1660.
[20] Yu WJ, Zhao JC, Luo HX, Shi JY, Zhang DX. Experimental study on mechanical behavior of an impacted steel tubular T-joint in fire. J Constr Steel Res 2011; 67: 1376-1385.
[21] Chen C, Shao YB, Yang J. Experimental and numerical study on fire resistance of circular tubular T-joints. J Constr Steel Res 2013; 85: 24-39.
[22] Yang J, Shao YB, Chen C. Experimental study on fire resistance of square hollow section (SHS) tubular T-joint under axial compression. Adv Steel Constr 2014; 10(1): 72-84.
[23] He SB, Shao YB, Zhang HY, Yang DP, Long FL. Experimental study on circular hollow section (CHS) tubular K-joints at elevated temperature. Eng Fail Anal 2013; 34: 204-216.
[24] He SB, Shao YB, Zhang HY, Wang QL. Parametric study on performance of circular tubular K-joints at elevated temperature. Fire Safety J, 2015; 71: 174-186.
[25] He SB, Shao YB, Zhang HY. Evaluation on fire resistance of tubular K-joints based on critical temperature method. J Constr Steel Res 2015; 115: 398-406.
[26] Gao F, Guan XQ, Zhu HP, Liu XN. Fire resistance behaviour of tubular T-joints reinforced with collar plates. J Constr Steel Res, 2015; 115: 106-120.
[27] Gao F, Zhu HP, Liu XN. Failure Behavior of Axially Loaded Tubular Y-Joints under Fire.

Adv Steel Constr, 2013; 16(9): 1523-1533.
[28] Chen C, Shao YB, Yang J. Study on fire resistance of circular hollow section (CHS) T-joint stiffened with internal rings. Thin-Walled Struct, 2015; 92: 104-114.
[29] Feng R, Young B. Design of cold-formed stainless steel tubular joints at elevated temperatures. Eng Struct 2012; 35: 188-202.
[30] Packer JA, Wardenier J, Zhao XL, van der Vegte A, Kurobane Y. Design guide for rectangular hollow section (RHS) joints under predominantly static loading. CIDECT, Verlag TUV Rheinland. Cologne, Germany, 2009.
[31] Lan XY, Huang Y. Structural design of cold-formed stainless steel tubular X- and T-joints at elevated temperatures. Thin-Walled Struct 2016; 108: 270-279.
[32] ABAQUS/Standard. Version 6.13-1. USA: K. a. S. Hibbit; 2013.
[33] Kurobane Y, Ogawa K, Ochi K, Makino Y. Local buckling of braces in tubular K-joints. Thin-Walled Struct 1986; 4: 23-40.
[34] Gho WM, Yang Y, Gao F. Failure mechanism of tubular CHS joints with complete overlap of braces. Thin-Walled Struct 2006; 44: 655-666.
[35] Fung TC, Soh CK, Gho WM, Qin F. Ultimate capacity of completely overlapped tubular joints I. An experimental investigation. J Constr Steel Res 2001; 57: 855-880.
[36] Rasmussen KJR. Full-range stress-strain curves for stainless steel alloys. J Constr Steel Res 2003; 59: 47-61.
[37] Fleischer O, Herion S, Puthli R. Numerical investigation on the static behaviour of CHS X joints made of high strength steels, Tubular Structures XII, Shanghai, 2008, 597-605.
[38] Lee MMK. Strength, stress, and fracture analyses of offshore tubular joints using finite elements. J Constr Steel Res 1999; 51: 265-286.
[39] Wang T, Hou C, Li W, Han LH, Rasmussen K. Analytical behaviour of concrete-filled steel tubular K-joints using stainless steel. in Proceedings of the Eighth International Conference on Steel and Aluminium Structures, Hong Kong, 2016.
[40] Chen J, Young B. Stress–strain curves for stainless steel at elevated temperatures. Eng Struct 2006; 28: 229-239.

Table 1

Gap K-joints used for validating FE models.

Specimen	Chord		Brace 1		Brace 2				
	d (mm)	t (mm)	d_1 (mm)	t_1 (mm)	d_2 (mm)	t_2 (mm)	g (mm)	θ_1 (°)	θ_2 (°)
KC48-30 [2]	101.5	2.80	48.0	2.92	48.0	2.92	87	29.2	30.0
KC48-45 [2]	103.0	2.84	48.2	2.92	48.2	2.92	29	44.0	44.5
KC76-30 [2]	101.0	2.79	72.3	2.94	72.3	2.94	24	29.5	30.0
G2C [33]	216.4	7.82	165.0	5.28	165.0	5.28	29.5	60	60

Table 2

Overlapped N-joints used for validating FE models.

Specimen	Chord		Through brace		Lap brace				
	d (mm)	t (mm)	d_1 (mm)	t_1 (mm)	d_2 (mm)	t_2 (mm)	g (mm)	θ_1 (°)	θ_2 (°)
N-joint [34]	219.1	7.9	168.3	7.1	88.9	5.5	143.0	90	30
N-joint [35]	457.2	12.7	273.1	9.3	168.3	7.1	85	90	45

Table 3

Material properties of specimens for validation study.

Specimen	Member	E_0 (GPa)	f_y (MPa)	f_u (MPa)	ε_u (%)
KC48-30 [2]	Chord/Brace	190	395	640	38.3
KC48-45 [2]	Chord/Brace	190	395	640	38.3
KC76-30 [2]	Chord/Brace	190	395	640	38.3
G2C [33]	Chord	210	480	532	10.0
	Brace	210	363	436	10.0
N-joint [34]	Chord	199	361	462	10.0
	Through brace	201	403	519	10.0
	Lap brace	193	380	469	10.0
N-joint [35]	Chord	191	377	472	10.0
	Through brace	197	374	457	10.0
	Lap brace	205	386	477	10.0

Table 4

Comparison of peak loads.

Specimen	Mesh size (mm)	N_{FE} (kN)	N_{Test} (kN)	N_{FE}/N_{Test}
KC48-30 [2]	4	99.0	110.0	0.90
KC48-45 [2]	4	84.6	84.8	1.00
KC76-30 [2]	4	156.4	172.0	0.91
G2C [33]	8	799.9	830.8	0.96
N-joint [34]	5	360.3	380.5	0.95
N-joint [35]	8	1023.3	980.0	1.04
			Mean	0.96
			COV	0.056

Table 5

Parameters for gap K- and N-joints.

Joint number	Chord		Brace 1		Brace 2				
	d (mm)	t (mm)	d_1 (mm)	t_1 (mm)	d_2 (mm)	t_2 (mm)	g (mm)	θ_2 (°)	n
1	200	10	60	10	60	10	50	45	0
2	200	10	100	10	100	10	50	45	0
3	200	10	140	10	140	10	50	45	0
4	200	10	180	10	180	10	50	45	0
5	200	20	100	20	100	20	50	45	0
6	200	7	100	7	100	7	50	45	0
7	200	5	100	5	100	5	50	45	0
8	200	4	100	4	100	4	50	45	0
9	200	10	100	10	100	10	50	30	0
10	200	10	100	10	100	10	50	60	0
11	200	10	100	10	100	10	50	45	0.2
12	200	10	100	10	100	10	50	45	0.4
13	200	10	100	10	100	10	50	45	0.6

Table 6

Parameters for completely overlapped N-joints.

Joint number	Chord		Through brace		Lap brace				
	d (mm)	t (mm)	d_1 (mm)	t_1 (mm)	d_2 (mm)	t_2 (mm)	g (mm)	θ_2 (°)	n
1	200	10	160	8	48	8	100	45	0
2	200	10	160	8	80	8	100	45	0
3	200	10	160	8	112	8	100	45	0
4	200	10	160	8	144	8	100	45	0
5	200	20	160	16	80	16	100	45	0
6	200	7	160	5.6	80	5.6	100	45	0
7	200	5	160	4	80	4	100	45	0
8	200	4	160	3.2	80	3.2	100	45	0
9	200	10	160	8	80	8	100	30	0
10	200	10	160	8	80	8	100	60	0
11	200	10	160	8	80	8	100	45	0.3
12	200	10	160	8	80	8	100	45	0.6

Table 7

Material parameters for stainless steel at room temperature (Feng and Young [3, 4]).

Steel type	E_0 (GPa)	f_p (MPa)	f_y (MPa)	f_u (MPa)	ε_u (%)
Duplex	208	167	536	766	30.0
HSA	194	147	497	761	34.7
AISI 304	200	140	392	696	43.7

Note: HSA denotes high strength austenitic.

Table 8

Statistical analysis of r_{si}.

Case studies	Gap K-joints	Gap N-joints	Overlapped N-joints
N	119	119	112
Max.	1.05	1.05	1.04
Min.	0.89	0.89	0.87
Mean	0.98	0.98	0.96
COV	0.04	0.04	0.04
e	3.70%	3.58%	4.58%
s	4.39%	4.30%	5.39%

Note: The values of r_{si} at T=22°C were excluded in the calculation of the values of Mean, COV, *e* and *s*.

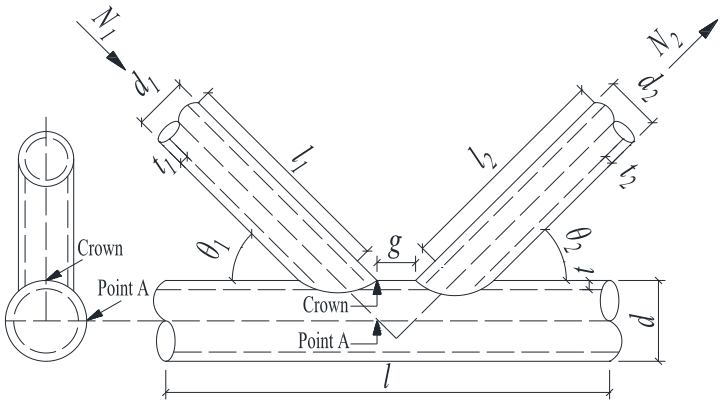

(a) Gap K-joints

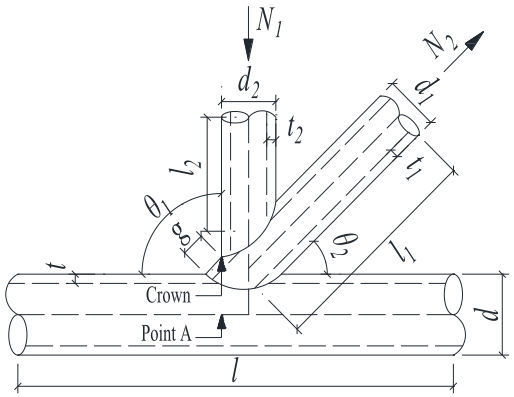

(b) Overlapped N-joints

Fig. 1. Configuration and notations of K- and N-joints.

(a) Gap K-joints (b) Overlapped N-joints

Fig. 2. Boundary condition and loading mode for validation study.

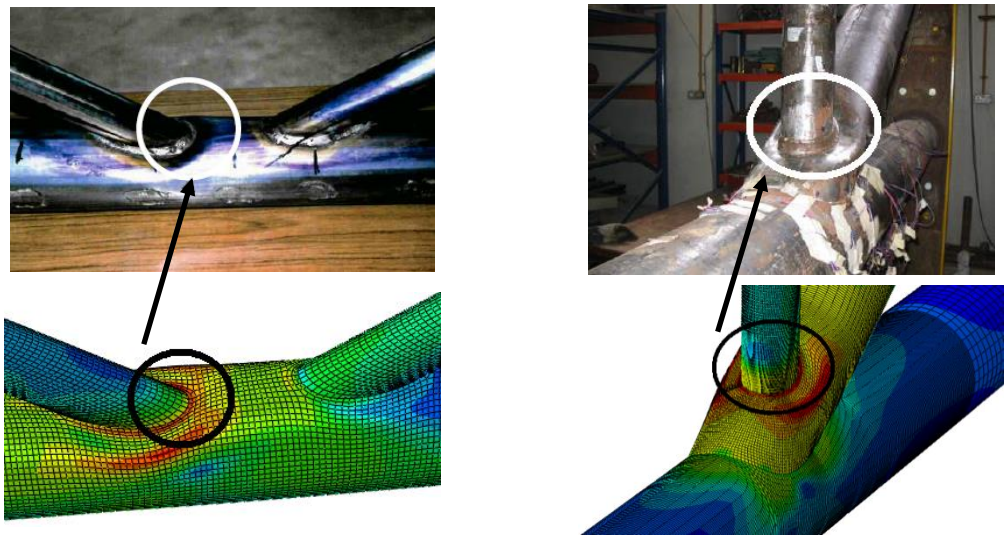

(a) KC48-30 [2, 39] (b) N-joint [34]

Fig. 3. Comparison of failure modes.

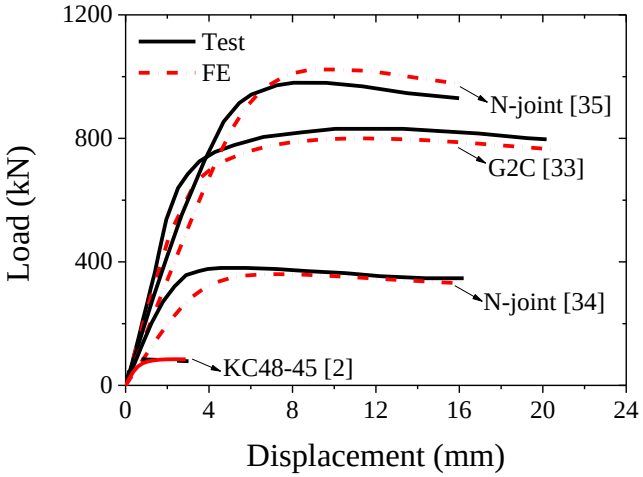

Fig. 4. Comparison of load-displacement curves.

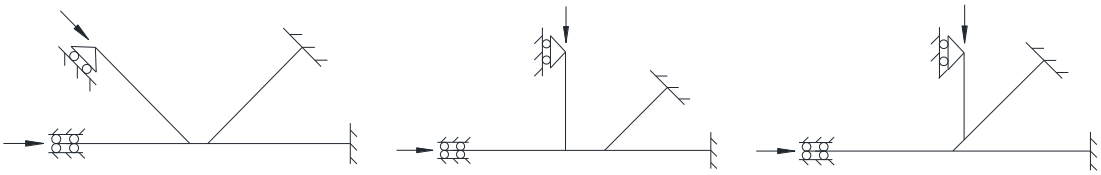

(a) Gap K-joints (b) Gap N-joints (c) Overlapped N-joints

Fig. 5. Boundary condition and loading mode for parametric study.

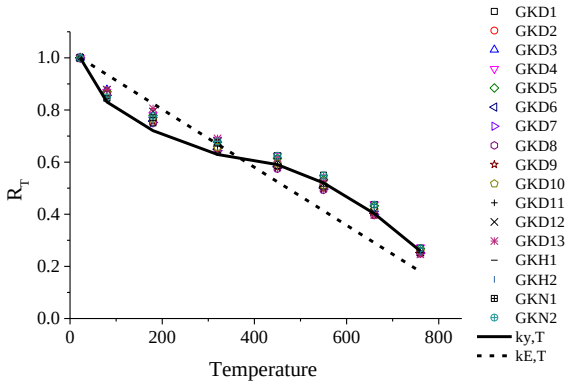

Fig. 6. Comparison for stainless steel gap K-joints.

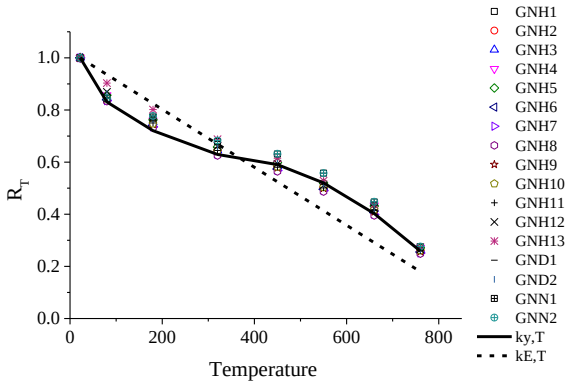

Fig. 7. Comparison for stainless steel gap N-joints.

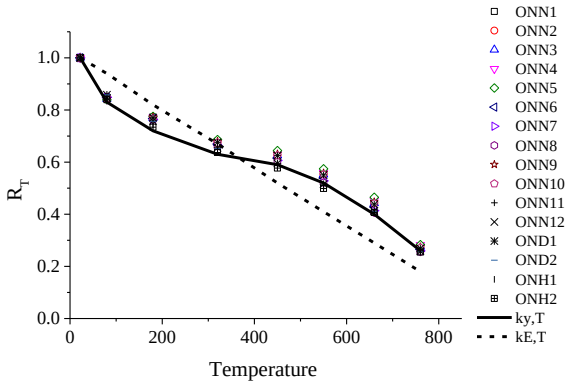

Fig. 8. Comparison for stainless steel overlapped N-joints.

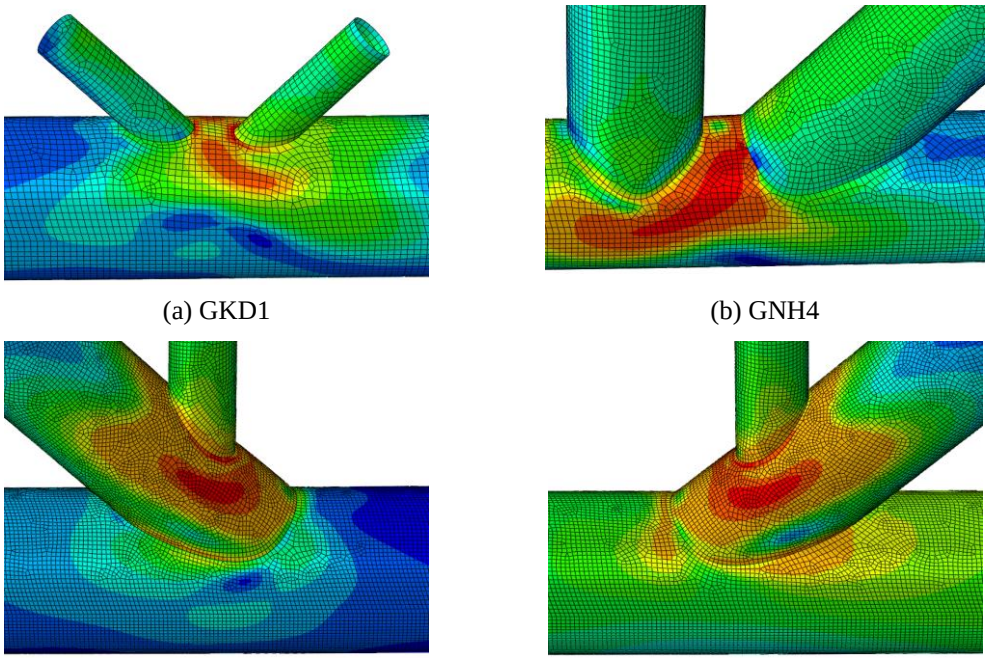

(a) GKD1 (b) GNH4

(c) ONN2 (d) ONN12

Fig. 9. Failure modes of K- and N-joints.